Half-Sandwich Iridium N-Heterocyclic Carbene Anticancer Complexes

Chuanlan Wang[†], Jinfeng Liu[†], Zhenzhen Tian, Meng Tian, Laijin Tian , Wenqian Zhao, Zhe Liu[*]

The Key Laboratory of Life-Organic Analysis and Key Laboratory of Pharmaceutical Intermediates and Analysis of Natural Medicine, Institute of Anticancer Agents Development and Theranostic Application, Department of Chemistry and Chemical Engineering, Qufu Normal University, Qufu 273165, China

Supporting Information

[†]The first two authors are equal first authors.

[*] Corresponding author.
E-mail:liuzheqd@163.com.

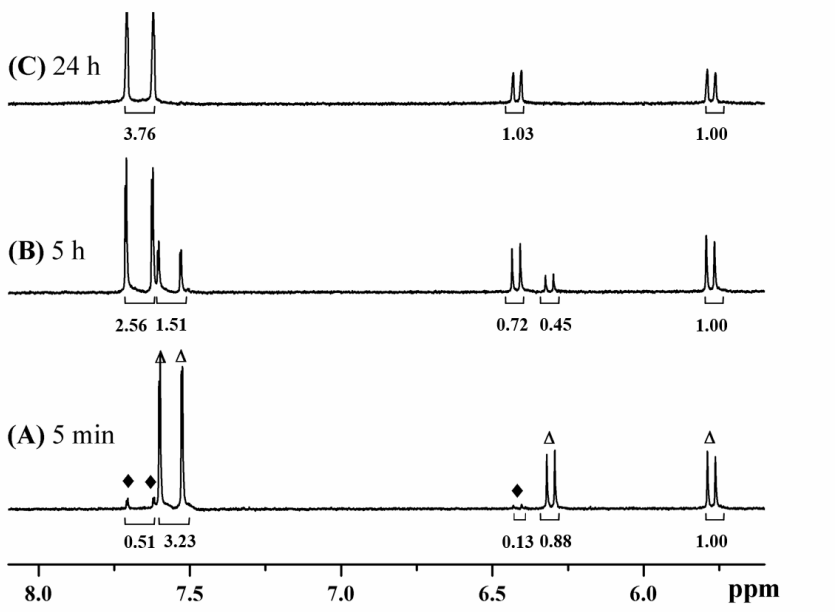

Figure S1. ^{1}H NMR spectra showing the hydrolysis of complex [(η^5-C_5Me_5)Ir(L1)Cl]PF_6 (**1A**) (1 mM) in 20% CD_3CN /80% D_2O (v/v) at 310 K. (A) after 5 min; (B) after 5 h ; (C) after 24 h. Peaks labeled ♦ correspond to aqua complex [(η^5-C_5Me_5)Ir(L1)D_2O]$^+$, and peaks labeled Δ correspond to complex [(η^5-C_5Me_5)Ir(L1)Cl]PF_6 (**1A**).

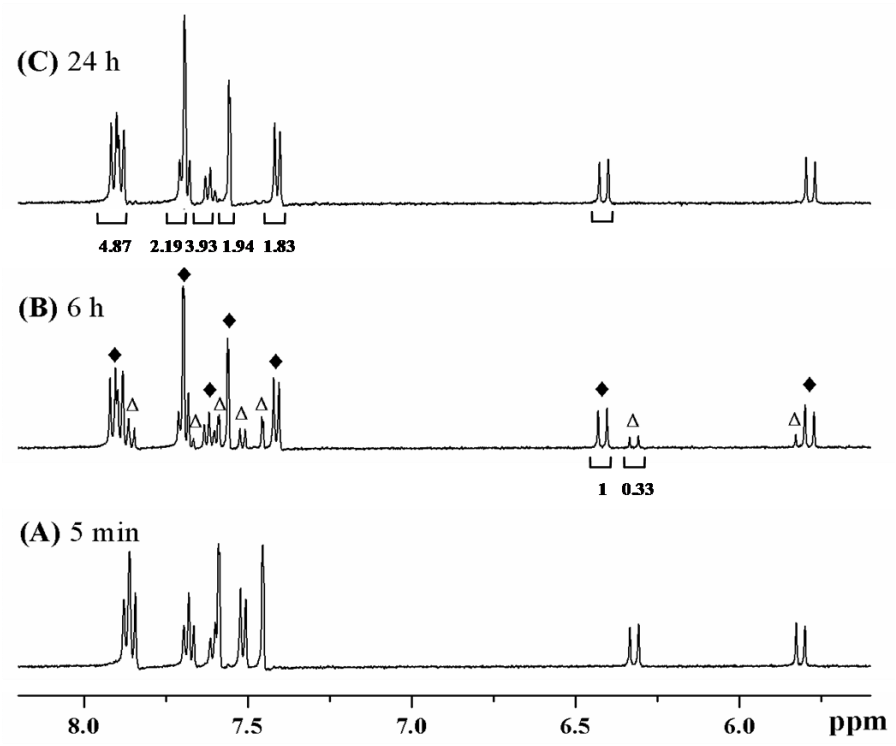

Figure S2. ^{1}H NMR spectra showing the hydrolysis of complex $[(\eta^5\text{-}C_5Me_4C_6H_4C_6H_5)Ir(L1)Cl]PF_6$ (**1C**) (1 mM) in 20% CD_3CN /80% D_2O (v/v) at 310 K. (A) after 5 min; (B) after 6 h; (C) after 24 h. Peaks labeled ♦ correspond to aqua complex $[(\eta^5\text{-}C_5Me_4C_6H_4C_6H_5)Ir(L1)D_2O]^+$, and peaks labeled Δ correspond to complex $[(\eta^5\text{-}C_5Me_4C_6H_4C_6H_5)Ir(L1)Cl]PF_6$ (**1C**).

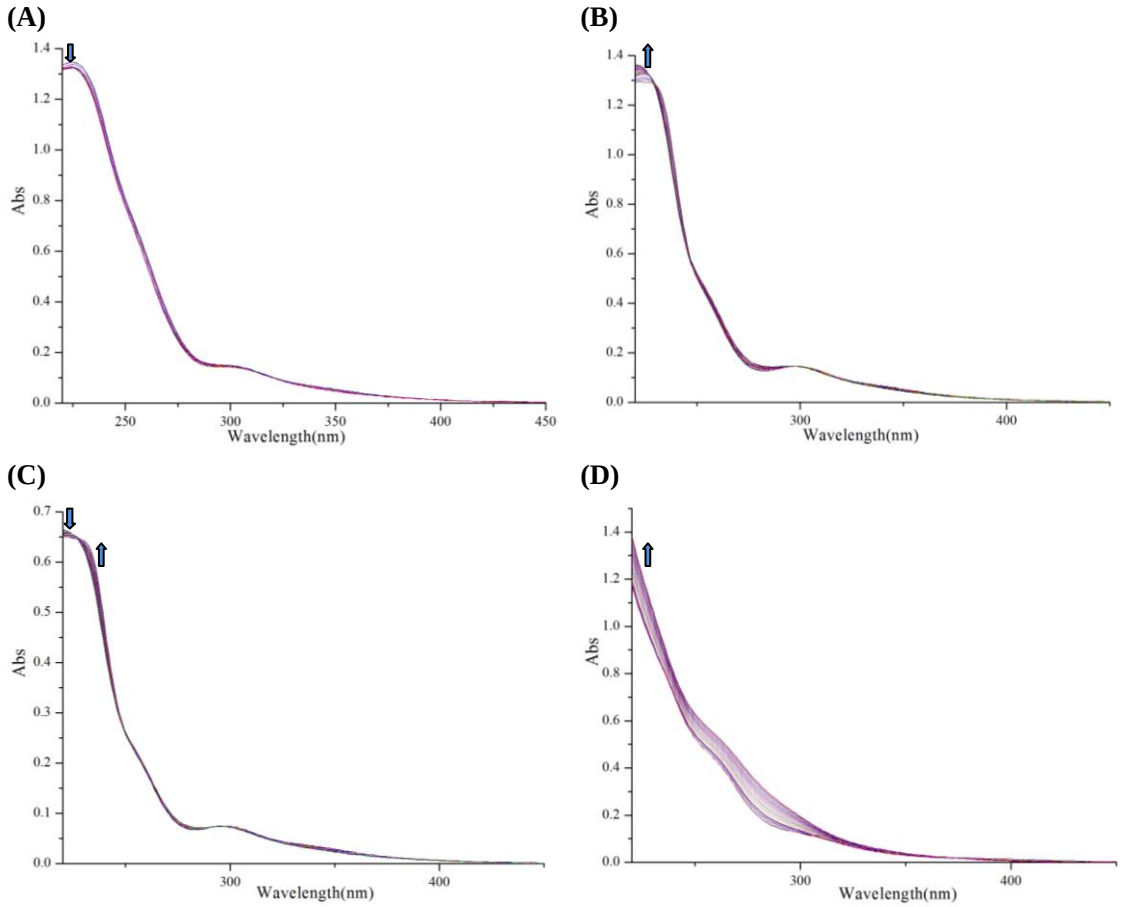

Figure S3. UV-Vis spectrum for a 50 μM solution of complexs (A) **1B**, (B) **2A**, (C) **3A**, (D) **4A** in 5% MeOH/95% H_2O (v/v) recorded over a period of 8 h at 298 K.

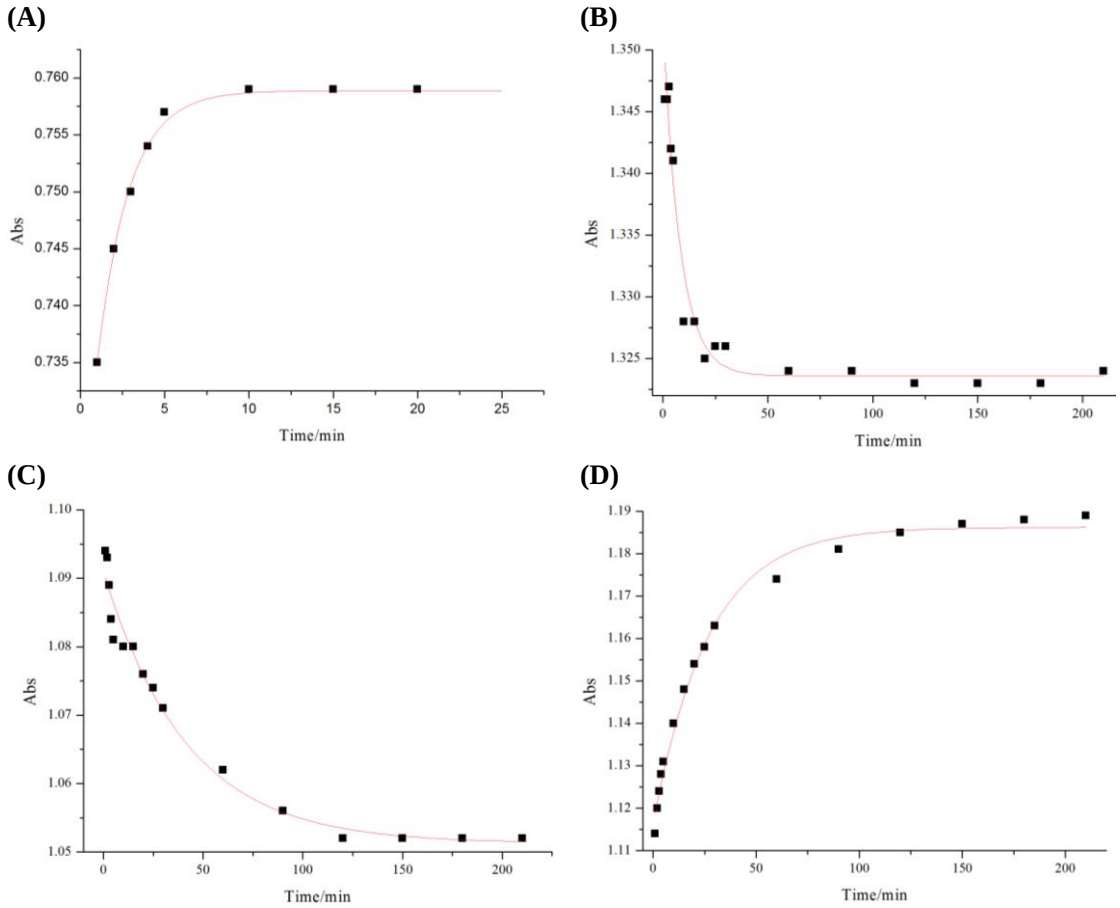

Figure S4. Time dependence of hydrolysis of (A) **1A**, (B) **1B**, (C) **1C** and (D) **2B** in 5% MeOH/95% H_2O (v/v) at 298 K based on UV-Vis spectrum by measuring the absorption difference at 224nm, 225nm, 243nm and 225nm, respectively.

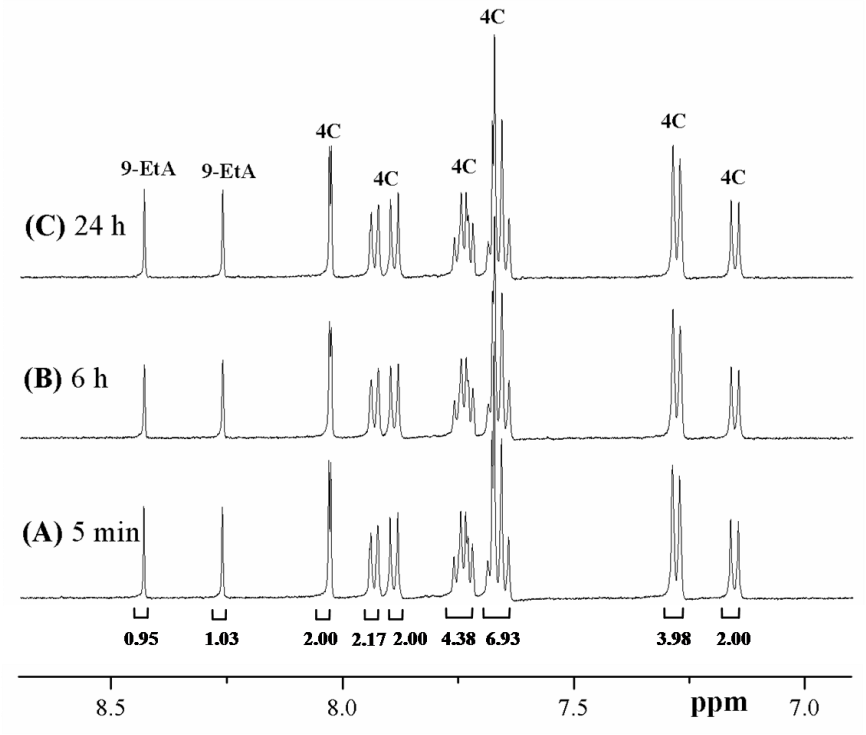

Figure S5. Reaction of $[(\eta^5\text{-}C_5Me_4C_6H_4C_6H_5)Ir(L4)Cl]PF_6$ **(4C)** with 9-ethyladenine. **(A)** ^1H NMR spectrum of an equilibrium solution of complex **4C** (1.0 mM) in 20% CD_3CN /80% D_2O (v/v) at 310 K, 5 min after the addition of 1 mol equiv 9-ethyladenine, **(B)** 6 h after addition of 1 mol equiv 9-ethyladenine at 310 K, and **(C)** 24 h after addition of 1 mol equiv 9-ethyladenine at 310 K. After 24 h, no reaction is observed.

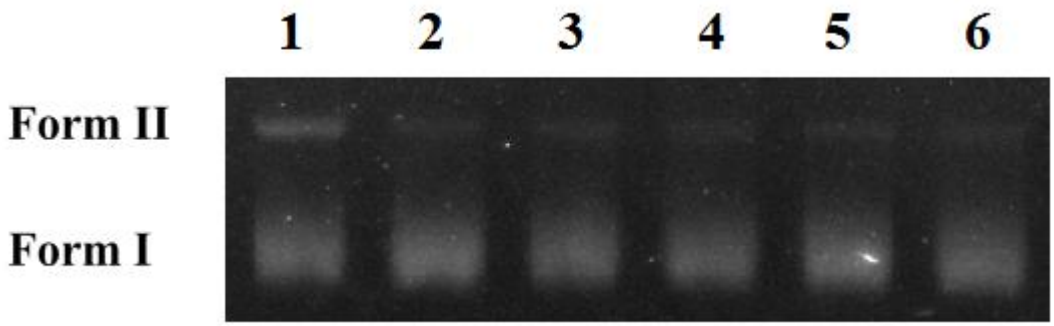

Figure S6. Agarose gel electrophoresis patterns for the cleavage of pBR322 DNA by various concentrations of complex **1B** cleavage conditions: 10 μM DNA; 1 mM Tris–CH_3COOH buffer; pH 8; 37℃ for 24h. Lane 1: DNA control; Lane 2: DNA + 20 μM **1B**; Lane 3: DNA +40 μM **1B**; Lane 4: DNA + 60 μM **1B**; Lane 5: DNA + 80 μM **1B**; Lane 6: DNA +100 μM **1B**.

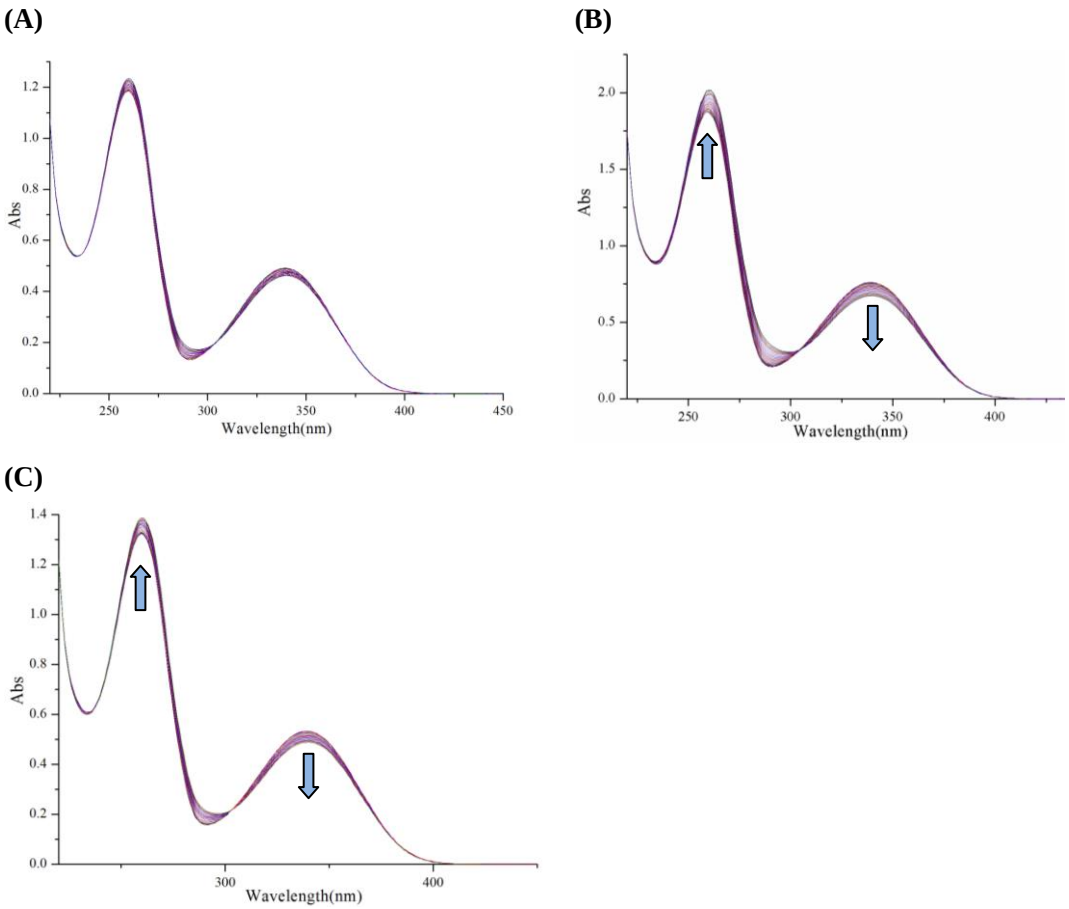

Figure S7. UV/Vis spectra of the reaction of NADH (87 μM) with **2B** and **2C** (0.8 μM) in MeOH/H_2O (5:95) at 298 K for 8 h. (A) control: only NADH; (B) **2B**; (C) **2C**.

Table S1. Extent of 9-EtG and 9-EtA Adduct Formation for Complexes **1A-4C** at 310 K after 24 h.

Complex	Cp^{X}	R	G adduct (%)	A adduct (%)
1A	Cp*	CH_3	0%	0%
1B	Cp^{xph}	CH_3	0%	0%
1C	Cp^{xbiph}	CH_3	0%	0%
2A	Cp*	CH_2CH_3	0%	0%
2B	Cp^{xph}	CH_2CH_3	0%	0%
2C	Cp^{xbiph}	CH_2CH_3	0%	0%
3A	Cp*	Bu	0%	0%
3B	Cp^{xph}	Bu	0%	0%
3C	Cp^{xbiph}	Bu	0%	0%
4A	Cp*	ph	0%	0%
4B	Cp^{xph}	ph	0%	0%
4C	Cp^{xbiph}	ph	0%	0%

Table S2. Flow cytometry analysis to determine the percentages of apoptotic cells, using Annexin V -FITC vs PI staining, after exposing Hela cells to complexes **2C** and **3C**.

Complex	Ir concentration	Population (%) Viable	Early apoptosis	Late apoptosis	Non-viable
2C	1 × IC_{50}	88.08 ± 0.1	1.18 ± 0.05	9.84 ± 0.7	0.90 ± 0.4
2C	2 × IC_{50}	14.93 ± 0.9	0.32 ± 0.1	83.17 ± 0.02	1.58 ± 0.9
3C	1 × IC_{50}	89.30 ± 0.8	0.79 ± 0.06	9.37 ± 0.1	0.55 ± 0.8
3C	2 × IC_{50}	75.56 ± 0.6	1.47 ± 0.2	21.85 ± 0.04	1.12 ± 0.3
control		95.32 ± 0.9	0.35 ± 0.1	3.70 ± 0.3	0.63 ± 0.6

Table S3. Cell cycle analysis carried out by flow cytometry using PI staining after exposing Hela cells to complexes **2C** and **3C**.

		Population (%)		
Complex	Ir concentration	G_1 phase	S phase	G_2/M phase
2C	0.25 × IC_{50}	46.0 ± 0.6	36.9 ± 0.1	14.0 ± 0.5
2C	0.5 × IC_{50}	51.0 ± 0.5	35.1 ± 0.3	13.5 ± 1
3C	0.25 × IC_{50}	52.6 ± 0.8	24.7 ± 0.7	21.7 ± 0.4
control		45.4 ± 0.7	37.7 ± 0.8	13.4 ± 0.1

Table S4. ROS induction in Hela cancer cells treated with complexes **2C** and **3C**.

Complex	Ir concentration	Population (%) Cells in low ROS levels	Cells in high ROS levels
2C	0.25 × IC_{50}	6.22 ± 0.2	93.54 ± 0.1
2C	0.5 × IC_{50}	6.15 ± 0.2	93.05 ± 0.7
3C	0.25 × IC_{50}	7.35 ± 0.5	95.42 ± 3
3C	0.5 × IC_{50}	4.52 ± 0.6	93.62 ± 0.3
Untreated cells (**negative control**)		99.13 ± 0.5	0.72 ± 0.6
CCCP treated cells (**positive control**)		20.79 ± 0.7	78.71 ± 1.7

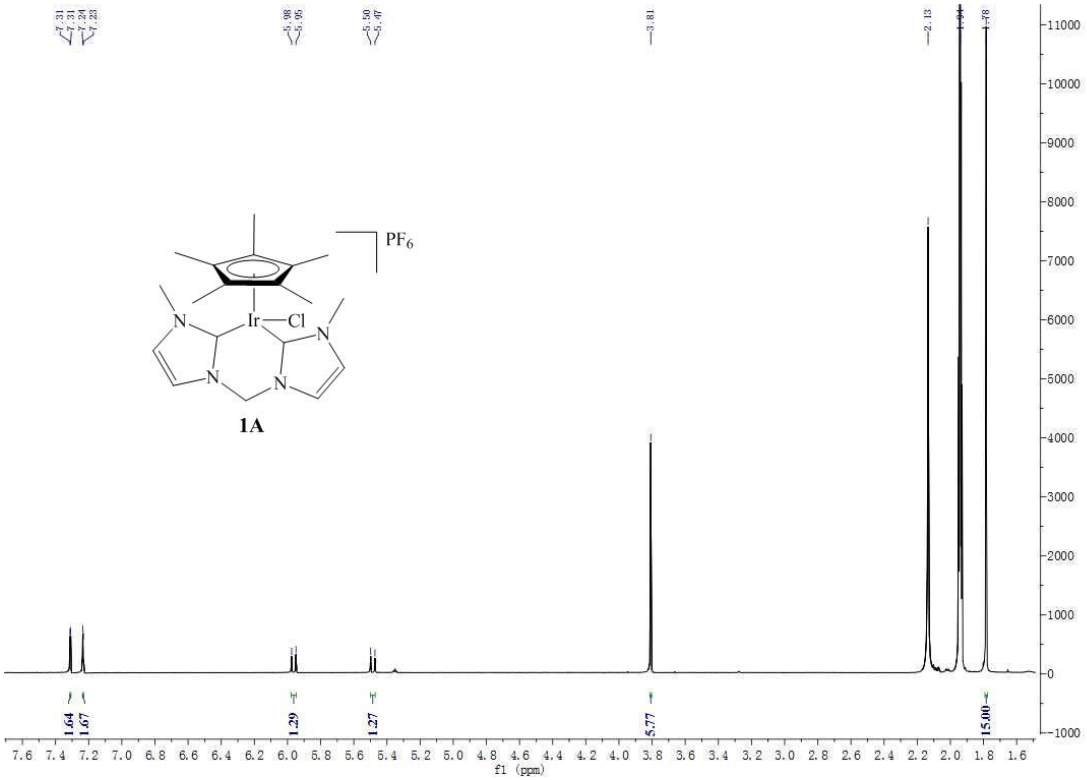

Figure S8: The ^{1}H NMR (500.13 MHz, CD_3CN) peak integrals of complex **1A** $[(\eta^5\text{-}C_5Me_5)Ir(L1)Cl]PF_6$.

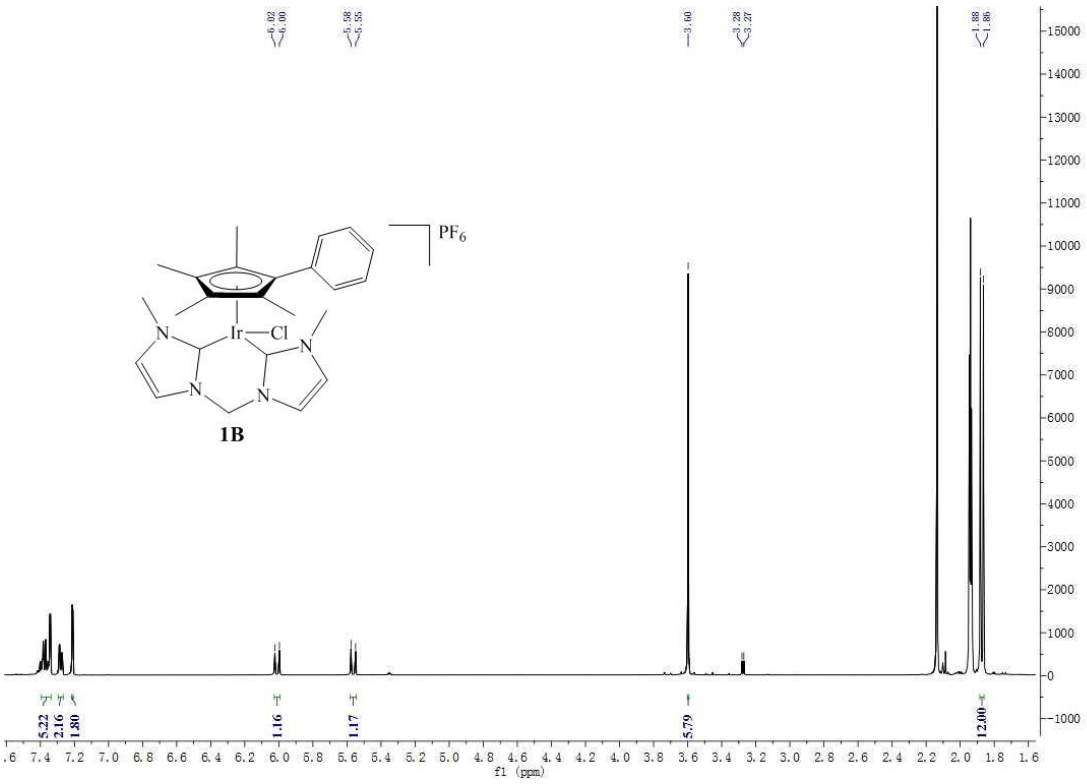

Figure S9: The ^{1}H NMR (500.13 MHz, CD_3CN) peak integrals of complex **1B** $[(\eta^5\text{-}C_5Me_4C_6H_5)Ir(L1)Cl]PF_6$.

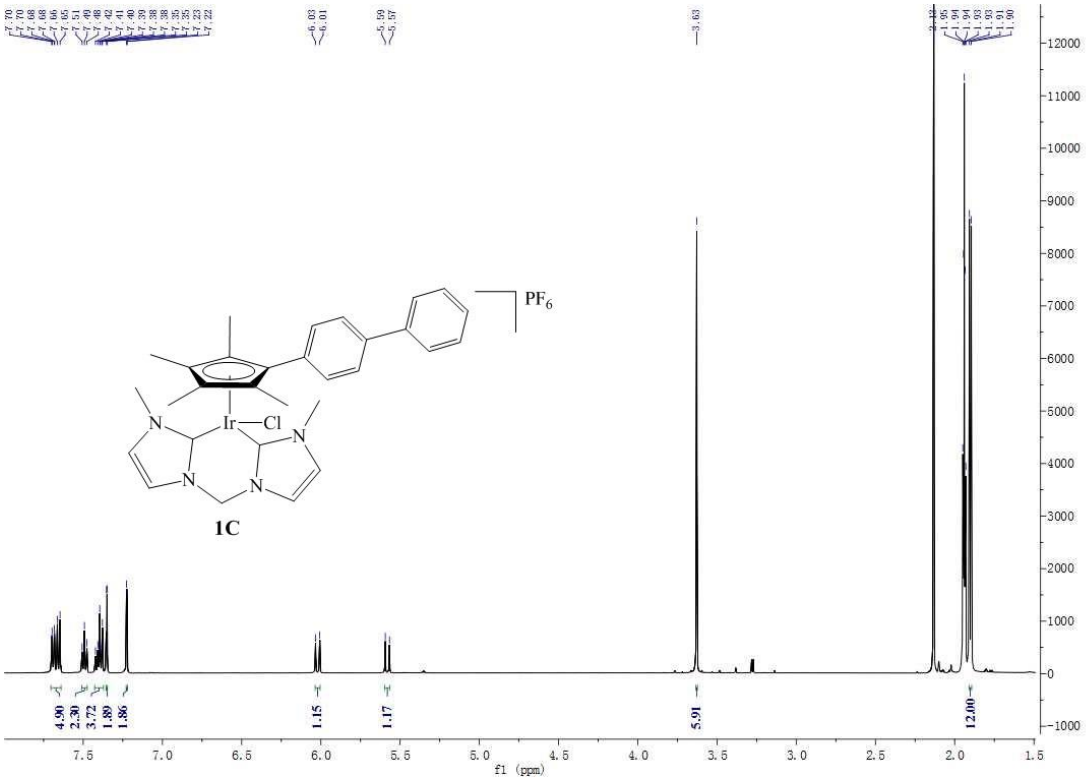

Figure S10: The ^{1}H NMR (500.13 MHz, CD_3CN) peak integrals at 295 K of complex **1C** $[(\eta^5\text{-}C_5Me_4C_6H_4C_6H_5)Ir(L1)Cl]PF_6$.

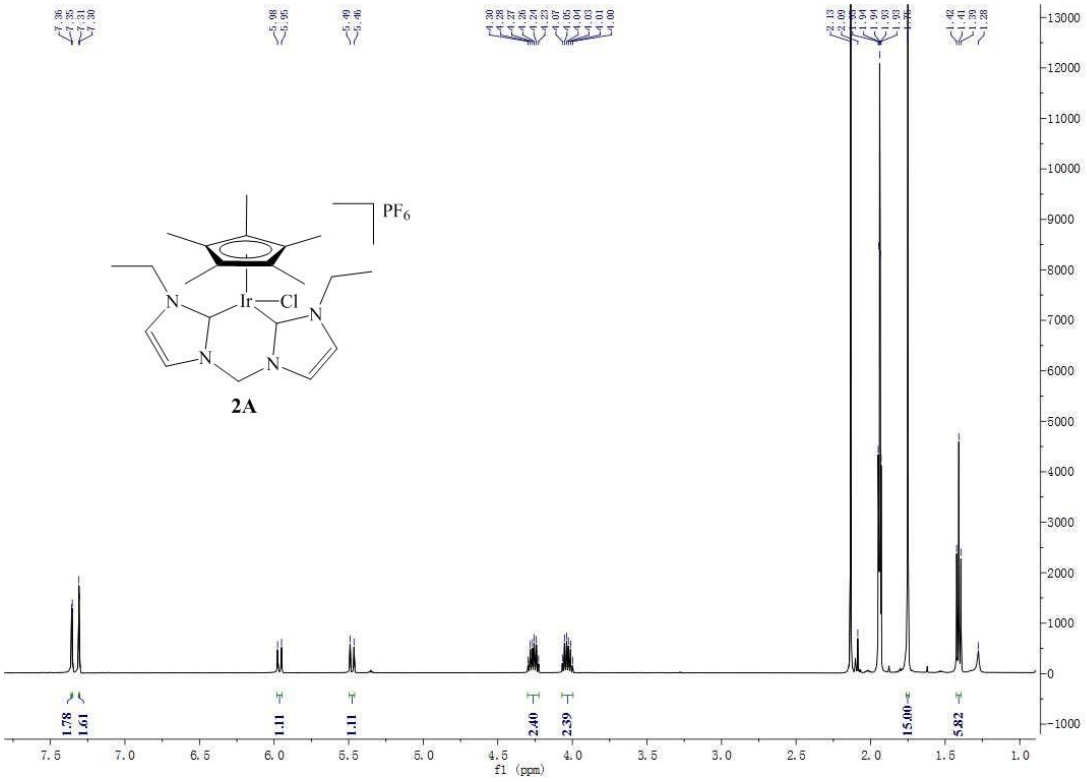

Figure S11: The ^{1}H NMR (500.13 MHz, CD_3CN) peak integrals at 295 K of complex **2A** $[(\eta^5\text{-}C_5Me_5)Ir(L2)Cl]PF_6$.

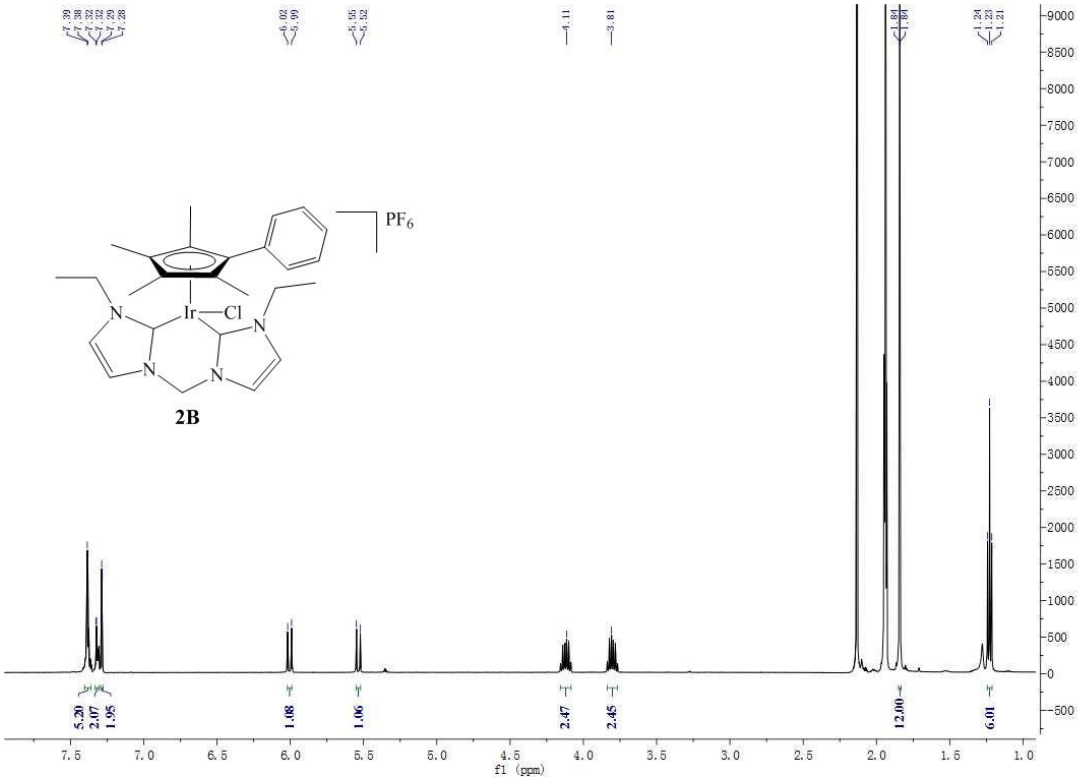

Figure S12: The ^{1}H NMR (500.13 MHz, CD_3CN) peak integrals at 295 K of complex **2B** $[(\eta^5\text{-}C_5Me_4C_6H_5)Ir(L2)Cl]PF_6$.

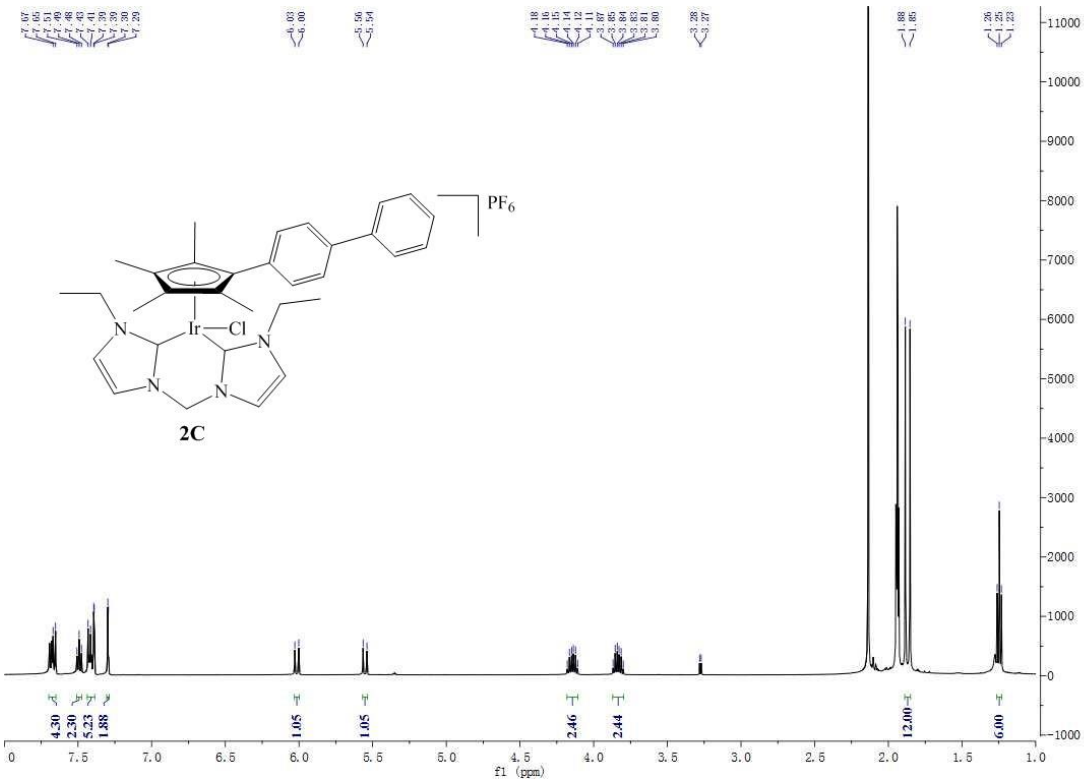

Figure S13: The ^{1}H NMR (500.13 MHz, CD_3CN) peak integrals at 295 K of complex **2C** $[(\eta^5\text{-}C_5Me_4C_6H_4C_6H_5)Ir(L2)Cl]PF_6$.

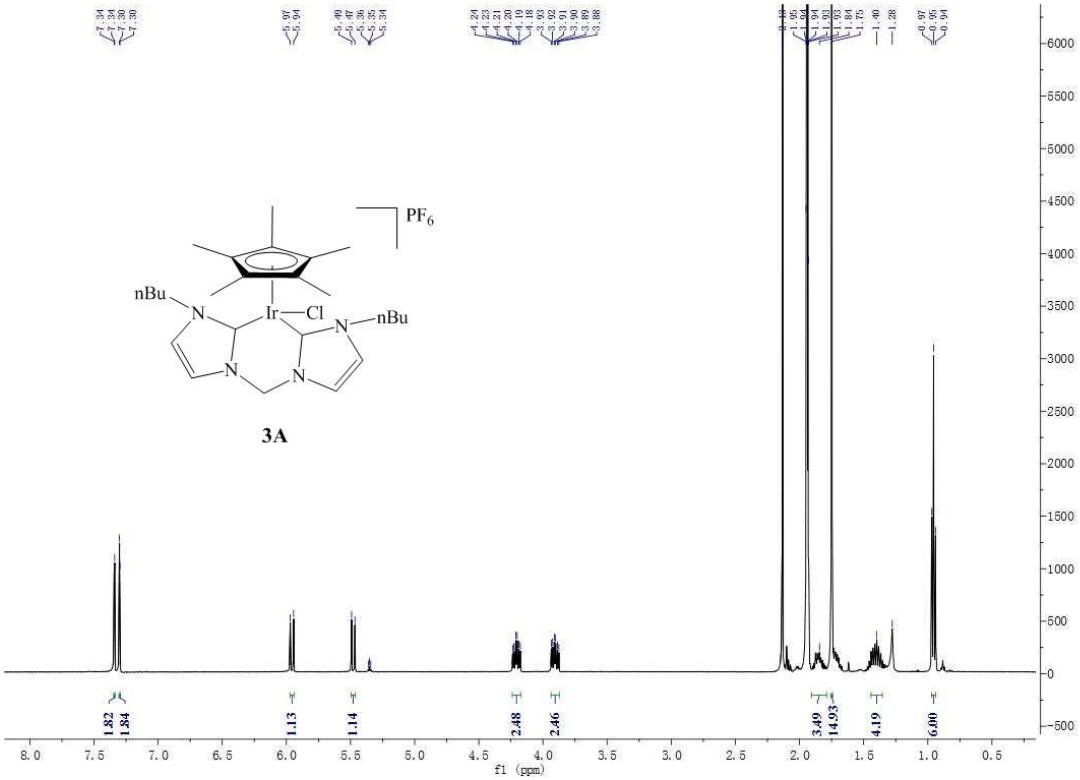

Figure S14: The ^{1}H NMR (500.13 MHz, CD_3CN) peak integrals at 295 K of complex **3A** [(η^5-C_5Me_5)Ir(L3)Cl]PF_6.

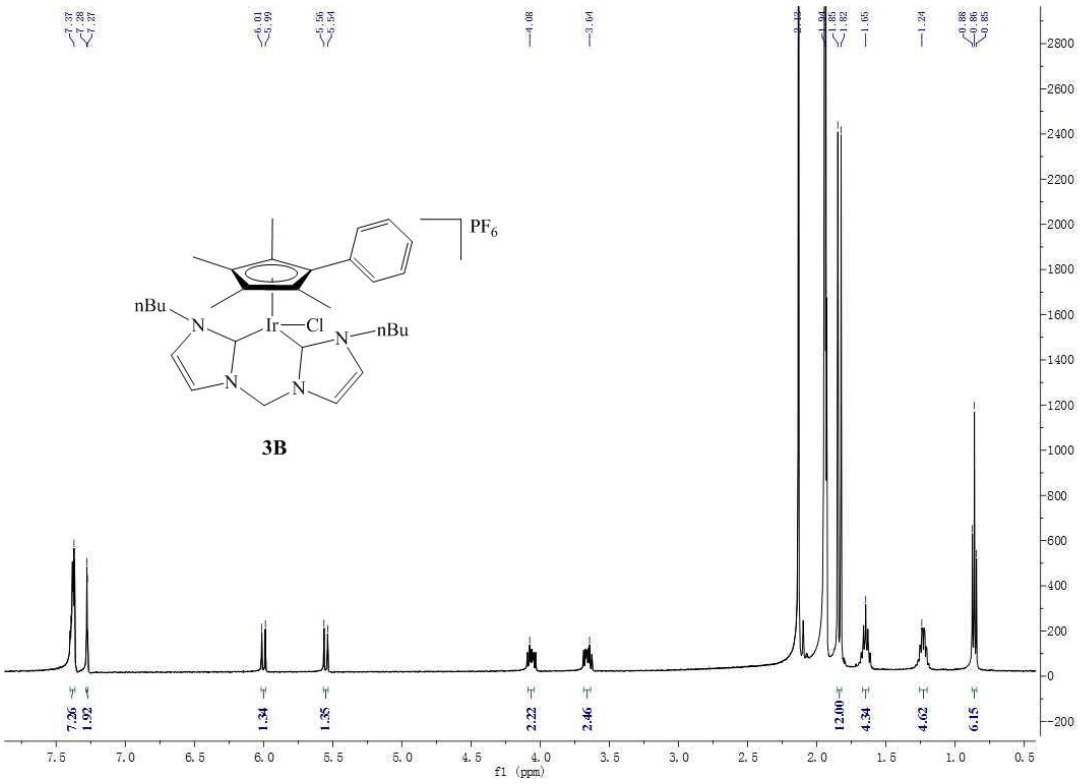

Figure S15: The ^{1}H NMR (500.13 MHz, CD_3CN) peak integrals at 295 K of complex **3B** [(η^5-$C_5Me_4C_6H_5$)Ir(L3)Cl]PF_6.

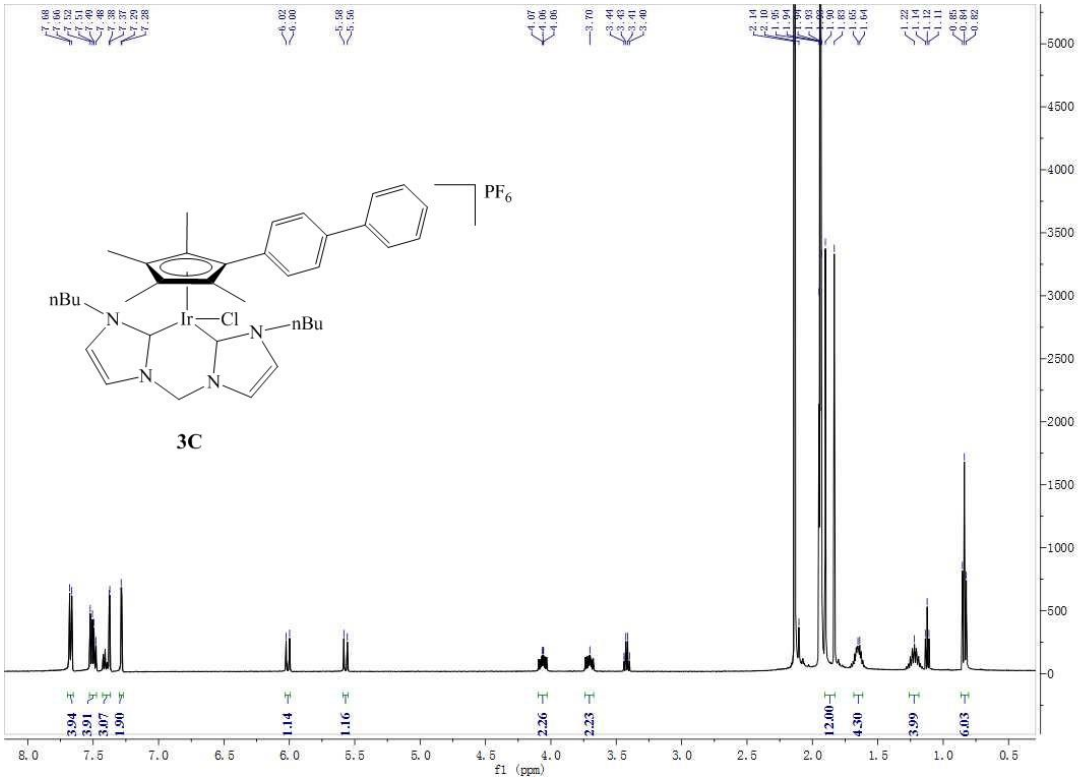

Figure S16: The ^{1}H NMR (500.13 MHz, CD_3CN) peak integrals at 295 K of complex **3C** $[(\eta^5\text{-}C_5Me_4C_6H_4C_6H_5)Ir(L3)Cl]PF_6$.

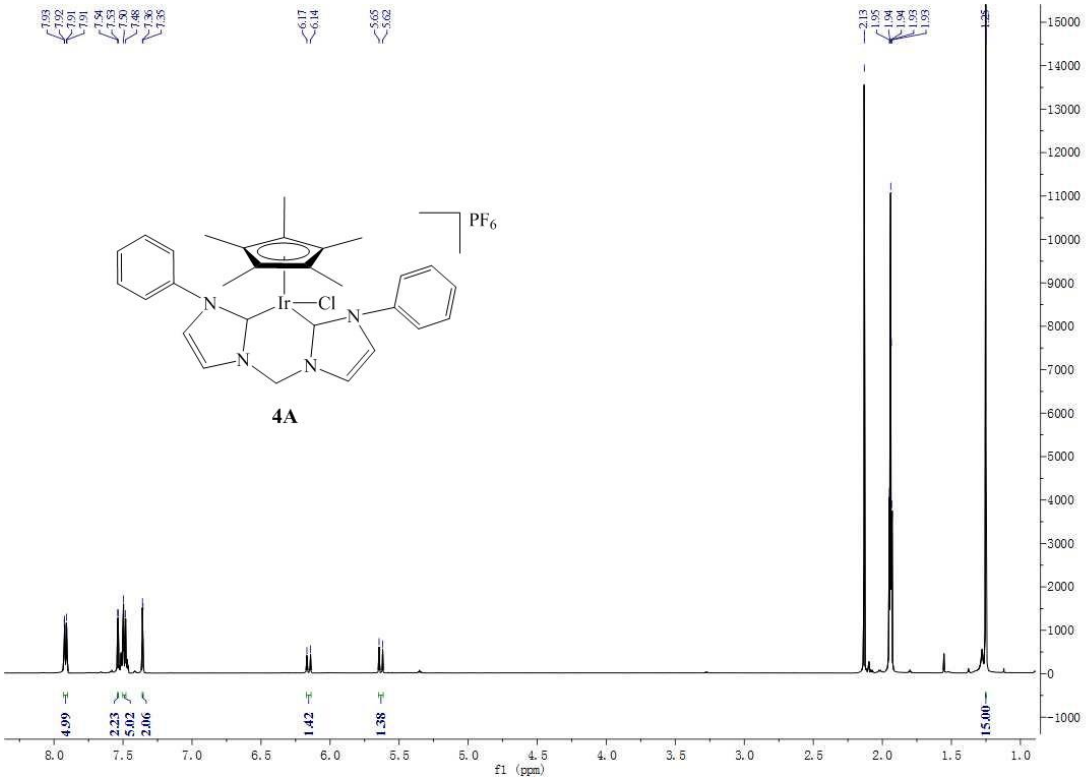

Figure S17: The ^{1}H NMR (500.13 MHz, CD_3CN) peak integrals at 295 K of complex **4A** $[(\eta^5\text{-}C_5Me_5)Ir(L4)Cl]PF_6$.

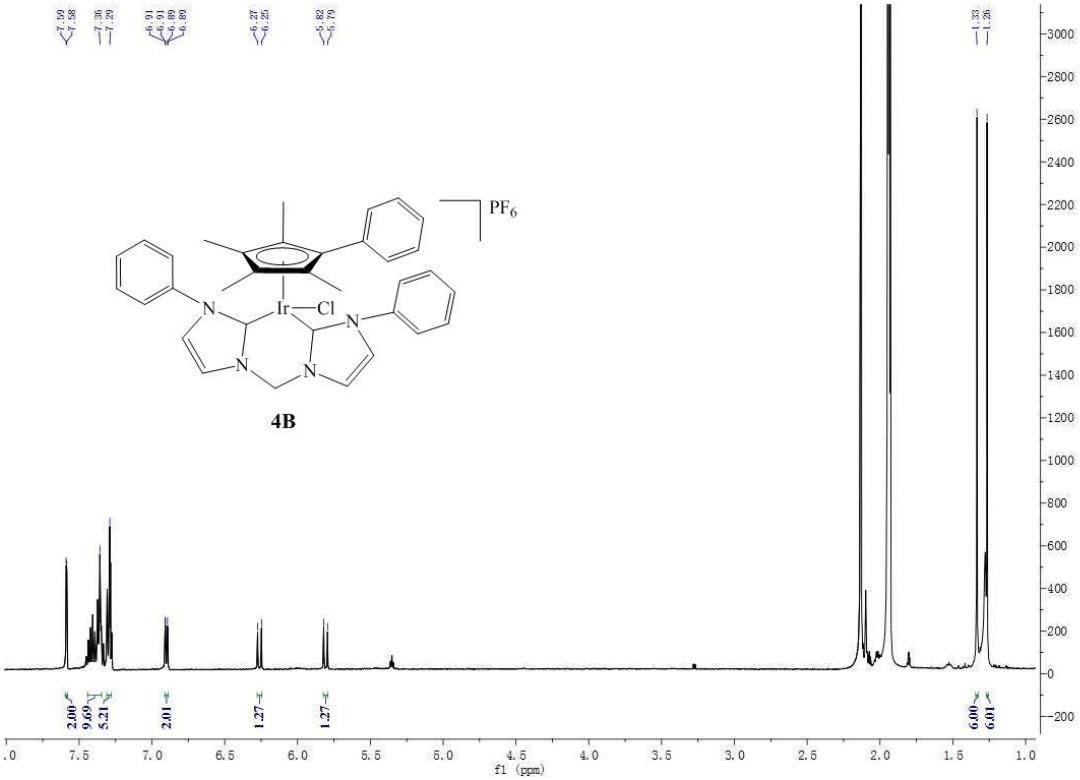

Figure S18: The ^{1}H NMR (500.13 MHz, CD_3CN) peak integrals at 295 K of complex **4B** $[(\eta^5\text{-}C_5Me_4C_6H_5)Ir(L4)Cl]PF_6$.

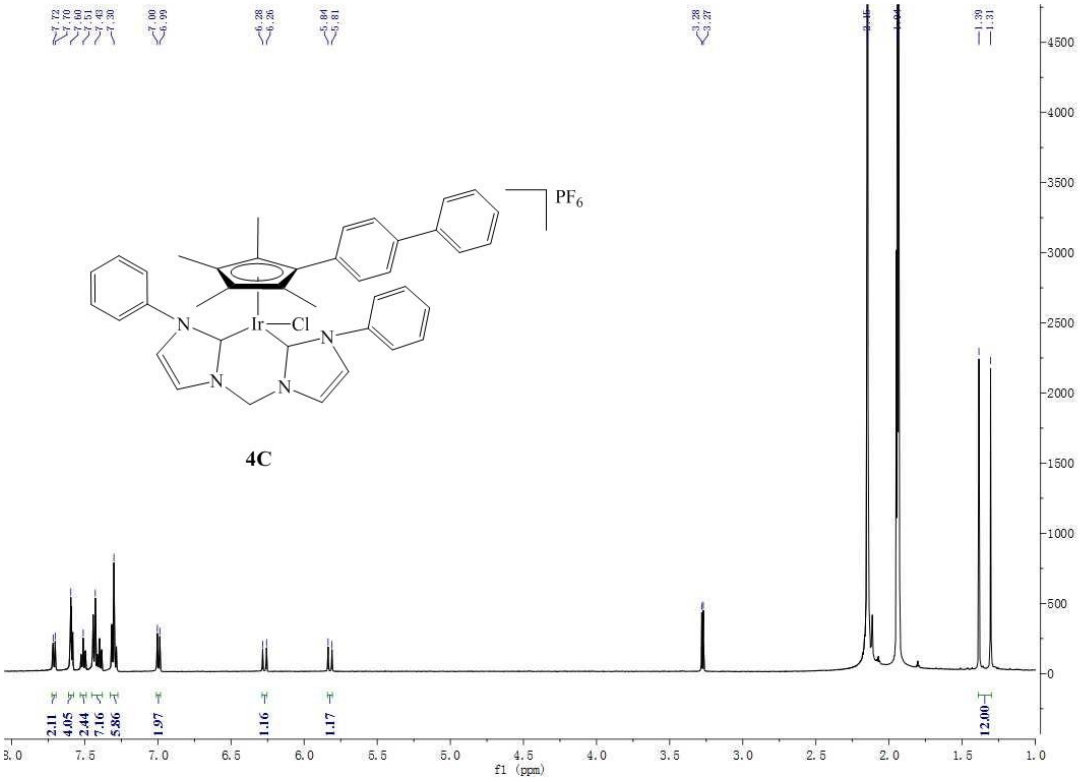

Figure S19: The ^{1}H NMR (500.13 MHz, CD_3CN) peak integrals at 295 K of complex **4C** $[(\eta^5\text{-}C_5Me_4C_6H_4C_6H_5)Ir(L4)Cl]PF_6$.

1A

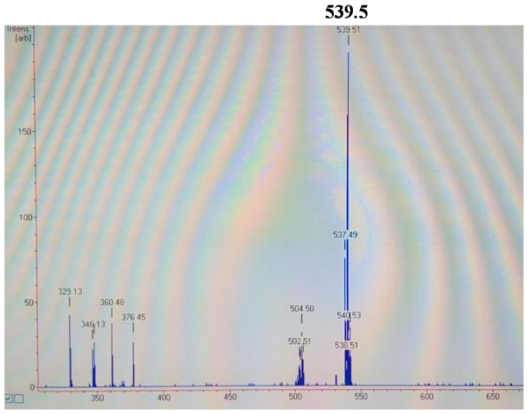

1B

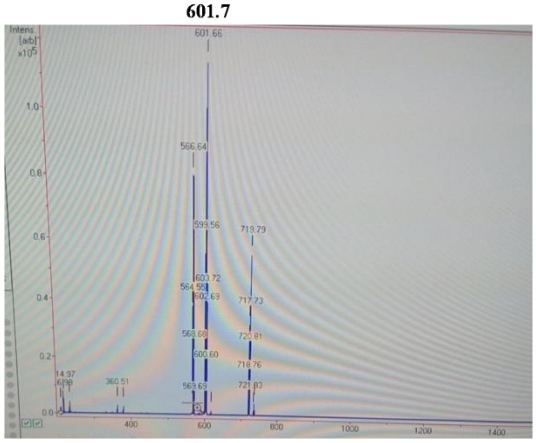

1C

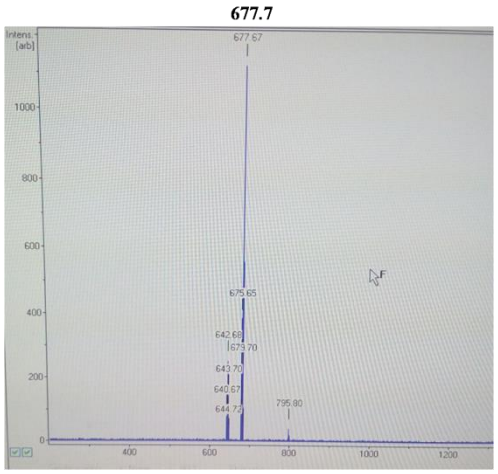

2A

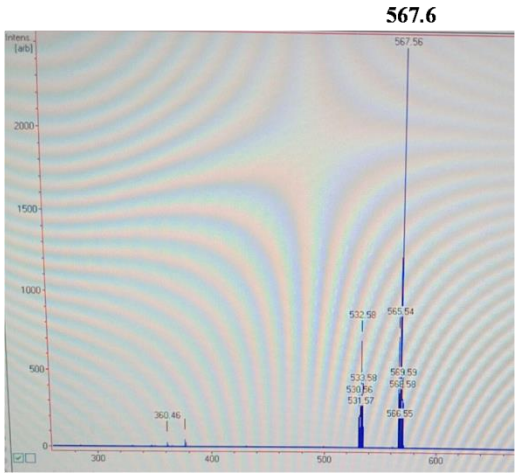

2B

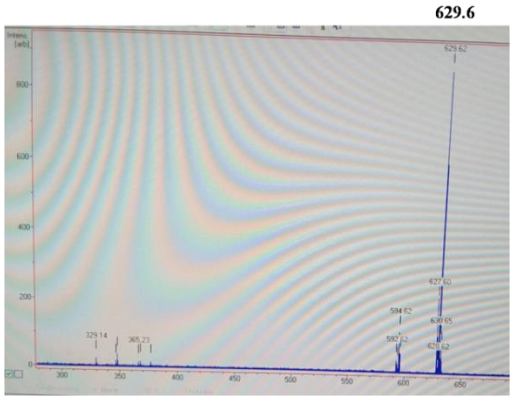

2C

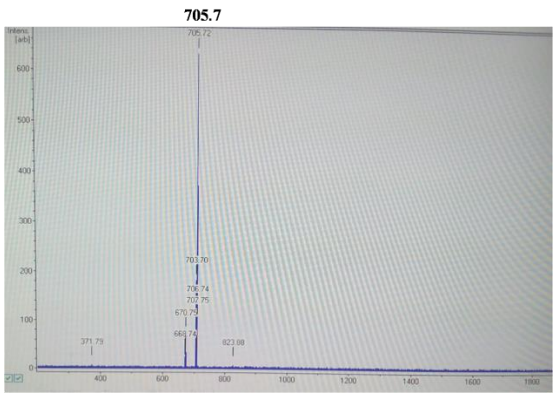

3A

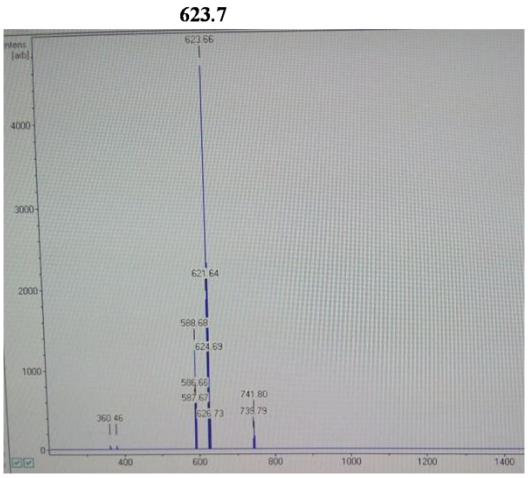

3B

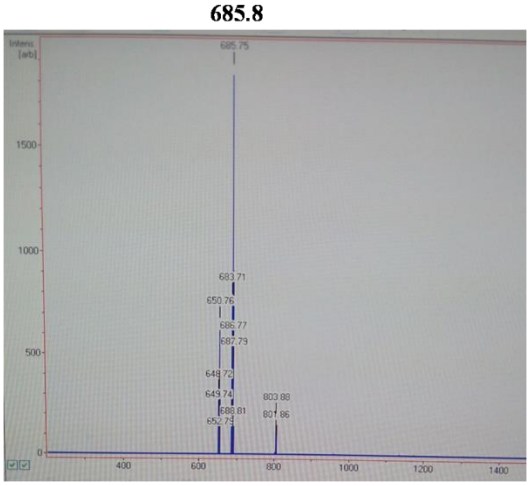

3C

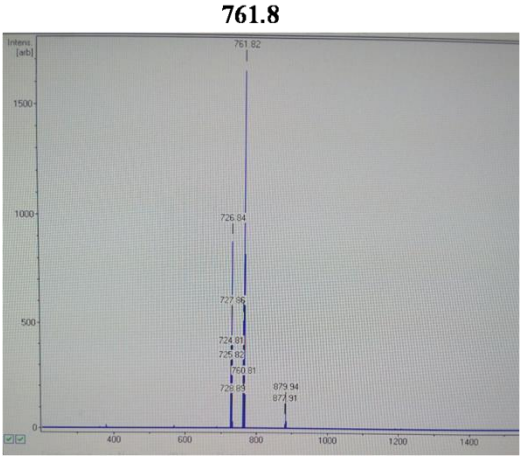

4A

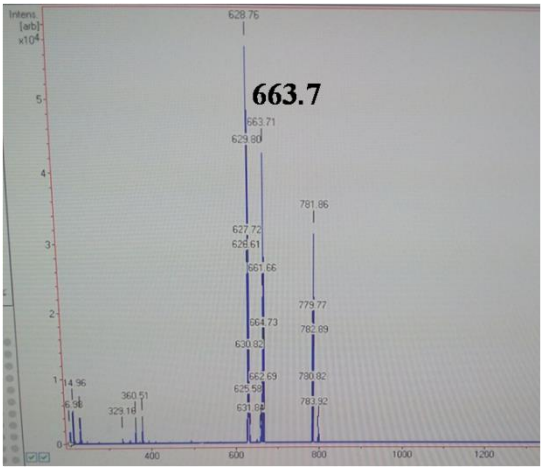

4B

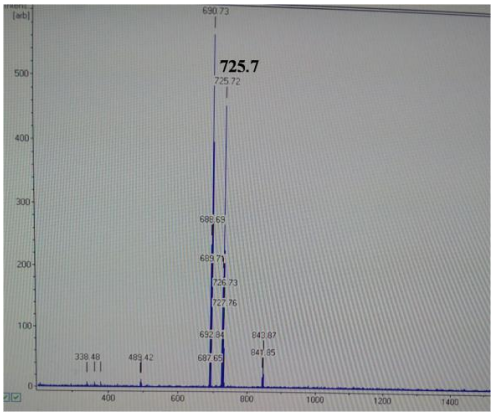

4C

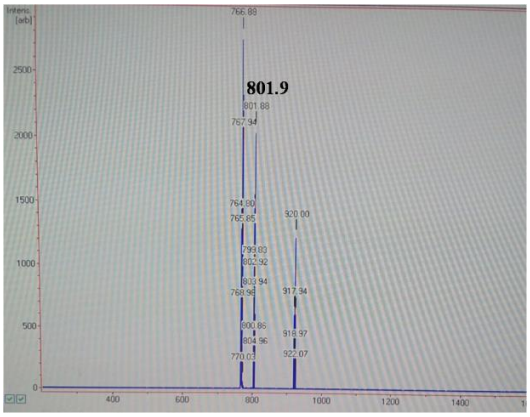

Figure S20: The Mass spectra of complexes **1A**-**4C**.